Internal flow and spray characteristics of a pintle-type outwards opening piezo-injector

J. M. Nouri, A. Marchi Y. Yan and C. Arcoumanis

Centre for Energy and the Environment
School of Engineering and Mathematical
Sciences, City University, Northampton Square,
London, EC1V OHB, UK

*corresponding author: j.m.nouri@city.ac.uk

ABSTRACT

The near-nozzle exit flow and the spray structure generated by an enlarged model of a second-generation pintle-type outwards opening injector have been investigated under steady flow conditions as a function of the fluid flow-rate and needle lift. A high resolution CCD camera and high-speed video camera have been employed to provide high-magnification images of the internal near nozzle exit flow in order to identify the origin of string ligaments and droplet formation at the nozzle exit. The images of the flow around the nozzle seat area showed clearly that air was entrained from outside up to the nozzle seat area under certain flow operating conditions (at low cavitation number, CN), forming pockets of air inside the annular nozzle which seem to be the main cause for the breaking of the liquid film into strings as it emerges from the nozzle, with alternating thin and thick liquid filaments. As the flow rate increased, the air pockets were suppressed, reduced in size and pushed towards the exit of the nozzle, resulting in a smoother surface spray.

The results showed that the number of strings increased linearly, within the measured range, with liquid exit velocity and that the spray cone angle was smaller or larger than the nominal value depending on the attachment of air pockets to the cartridge or needle surfaces, respectively; these two distinctive small and large cone angles were found to be dominant at low and high lifts. Increasing the flow rate further to the level when CN exceeds the critical value, gave rise to pockets of vapour which started to emerge in the nozzle seat region, breaking up rapidly as they were convected towards the nozzle exit. Visualization of the near nozzle exit flow has confirmed the existence of air entrainment and cavitation as two different phenomena occurring at different operating conditions.

INTRODUCTION

The second-generation direct-injection gasoline engines (DISI) have adopted the spray-guided concept which depends entirely on the spray dynamics and offers substantial improvements in terms of fuel economy, cycle efficiency and lower HC and CO_2 emissions, thus meeting the stringent emission targets set by the European Commission. This new combustion strategy which attracted even more the attention of the automotive manufacturers due to the worldwide concern for global warming and climate change, offers significant potential for overall leaner combustion, less cylinder-to-cylinder air–fuel variations and lower unburned hydrocarbon emissions particularly during cold start [1,2]. Well controlled stratified charge operation during part loads remains the key to the success of the DISI technology and it is achievable with this combustion concept since the spray-guided technique uses the dynamics of the injection process rather than the charge motion or piston wall to ensure that a combustible mixture reaches the spark plug at the time of ignition. Thus, to ensure the success of the new design, detailed knowledge of the fuel injection system and, in particular, the repeatability of the internal nozzle flow and spray characteristics become a prerequisite which has encouraged further research and development of this new gasoline direct-injection engine concept.

Currently, there are two mixture preparation strategies under development for spray-guided systems employing multi-hole and outwards opening pintle nozzles. In both cases, the prime objective is to avoid cycle-to-cycle spray variations so that a stable combustible mixture is formed prior to ignition which, in turn, depends on the internal nozzle flow characteristics including cavitation. The in-nozzle flow and spray characteristics of multi-hole injectors have been the subject of previous investigations [3-6]. Recently, intensive research has revealed that the outwards opening design offers many advantages, amongst those that it prevents the formation of the pre-spray associated with pressure-swirl atomizers and most inwards opening injectors. The major advantage of pintle-type injectors is that, under all operating conditions, the thickness of the initial liquid sheet formed at the nozzle exit is determined primarily by the needle lift (pintle stroke). This provides a flexible design tool that allows the spray angle, tip penetration and droplet size to be accurately controlled. Also, according to the manufacturing requirements, the absence of tiny nozzle holes being directly exposed to the hostile combustion chamber environment makes the outwards opening design more robust and cocking-free, a significant advantage relative to multi-hole nozzles. Another advantage with piezo injectors lies in the good control of the fuel spray and the extremely rapid opening time of the needle,

which allows formation of a fuel-air mixture with the right stoichiometry and, thus, improved thermodynamic efficiency and reduced fuel consumption but with excellent engine performance.

The spray structure produced from outwards opening injectors has a hollow cone spray structure similar to the swirl pressure atomizer but detailed results about this type of injector are very limited. An early study [7] of spray visualisation using this injector, showed that the spray emerging from the nozzle does not contain the poorly atomized pre-spray identified with swirl injectors [8, 11] and that there were very small injection-to-injection variations of the spray cone angle. Close-up images of the spray in a recent investigation [12] showed that the annular spray jet had a distinctive surface structure with strings of fuel ligaments/droplets (see Figure 1) which were confirmed by Phase Doppler Anemometry (PDA) measurements; the string spacing was determined to be around 0.375 and 0.6 mm at 2.5 and 10 mm, respectively, from the nozzle exit. Their results also showed that the overall spray cone angle was almost independent of the back/cylinder-pressure, a significant advantage relative to swirl pressure atomisers, and that mean droplet diameters of up to 20 μm were identified in the core of the strings 10 mm away from the injector exit. This strings-type structure originating at the nozzle exit had been examined before by other researchers [13-15] who argued that string formation could be the result of the interaction between the airflow and the injected annular liquid film.

The experimental investigation of [16] aimed at identifying the origin of this string-type spray structure by visualising the internal nozzle and the near-nozzle exit flows of an enlarged transparent model of an outwards opening non-cavitating injector. The results show a very complex flow in the region above the nozzle seat with four separated jet flows originating from the square cross-section of the needle guide and four pairs of counter-rotating vortices, each pair confined between two adjacent jets. The counter-rotating vortices were highly unstable in both longitudinal and circumferential directions, with the latter influencing the spray outside the nozzle and causing a circumferential oscillation of the emerging spray. The magnified images of the flow just outside the nozzle exit showed in the streamwise direction a spray structure with interconnecting filaments as the liquid film is exposed to the air. The formation of these filaments can be due to a combination of the two-phase flow structure inside the nozzle hole and the interaction between the liquid jet dynamic force, surface tension force and aerodynamic force due to the air circulation through entrainment. The interspacing between the strings was found to be linearly related to injection velocity and almost independent of the needle lift within the range of tested experimental conditions.

Parallel to this investigation, CFD calculations of the spray and the internal nozzle flow reported in [17, 18] have confirmed most of the previous experimental findings. In particular, they showed the flow complexity upstream of the nozzle seat with unstable recirculation zones, which are known to result to the so-called 'collapsing' or 'opening' spray types. Their results also showed that the outside nozzle shape and the boundary conditions exert an influence on the emerging spray. Finally, better understanding was provided about the formation of the 'string' type spray structure produced by such nozzles which confirmed the experimental observations. It has thus been demonstrated that the formation of strings is linked to the formation of a two-phase flow inside the nozzle, either as a result of the initiation and development of cavitation or due to the incomplete filling by the fluid of the expanding annular needle seat flow passage, which induces air entrainment and leads to flow separation just upstream of the nozzle exit.

The present work is the continuation of the experimental study in [16] but in a cavitating nozzle geometry and its main objective is the characterisation of the internal nozzle flow and, in particular, the formation of the flow filaments near the nozzle exit. The internal flow was visualised and monitored with pulsed and continuous light sources, a high-resolution CCD camera and a high-speed video recorder. The following sections describe, in turn, the experimental arrangement and relevant instrumentation, the obtained results and a summary of the main conclusions.

FLOW ARRANGEMENT AND INSTRUMENTATION

The steady flow rig, which was similar to that presented in [3, 16], comprises two pumps, connected to the model injector at its inlet and outlet to provide the maximum pressure difference across the injector, a supply tank and an ultrasonic flow meter as shown in Figure 2. The large-scale model injector, made from acrylic (Perspex), is geometrically similar to the real size injector but 23.3 times larger. The water flow through the model injector was steady by fixing the needle at a given lift and pumping water through the model. Different steady-state operating conditions were tested as

a function of the flow rate and needle lift, but in all cases the Reynolds number was similar to that of the real injector at the nozzle exit in order to allow correlation of the model data to the real size injector. For the spray characterisation, water was injected into air, Figure 3(a), and subsequently collected in the open supply tank while for the cavitation study the water was injected into a Perspex chamber filled with water in order to visualise any formed water vapour, as shown in Figure 3(b). All the transparent parts, nozzle-block and the last section of the needle, as well as the lower chamber, have been manufactured from Perspex, while the rest of the needle and the needle casing (cartridge) were machined from stainless steel. At the inlet to the model injector a mixing chamber was installed, where water was fed in through four pipes equally spaced around the chamber to ensure thorough mixing and uniform flow into the model injector. These tests were carried out as a function of the flow rate and needle lift.
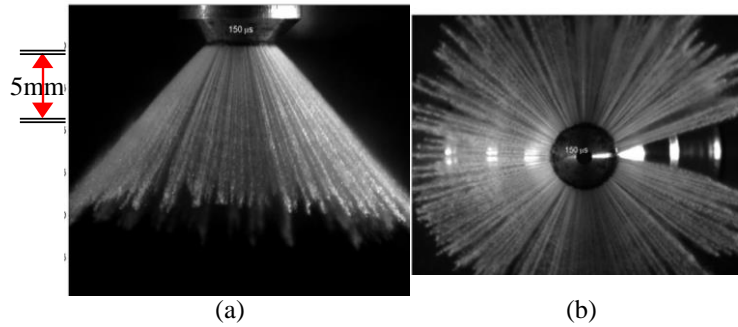

(a)	(b)

Figure 1: An example of spray images in a constant volume chamber at 150µs ASOI under atmospheric pressure, an injection duration of 0.33ms and injection pressure of 200bar [11]: (a) vertical plane, and (b) horizontal plane.
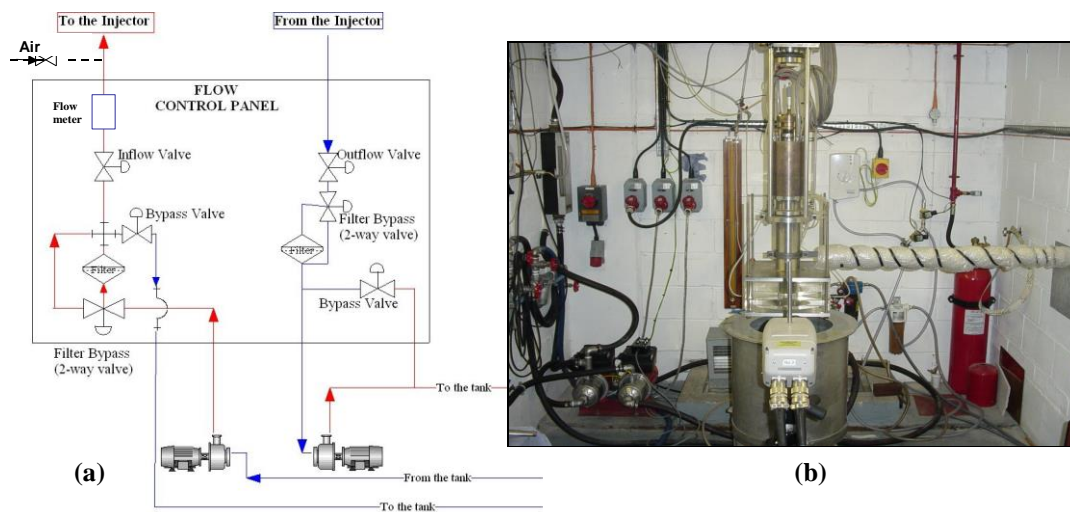

(a)	**(b)**

Figure 2: Flow arrangement: (a) schematic of the flow diagram showing the pumps, pipelines and valves; (b) flow rig set up.

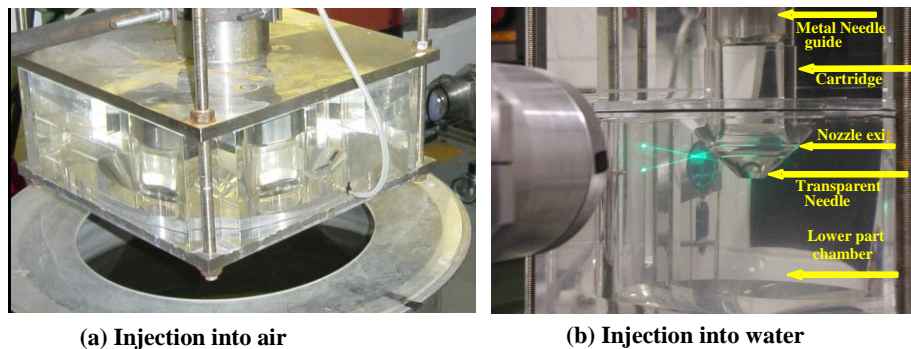|	
(a) Injection into air	**(b) Injection into water**

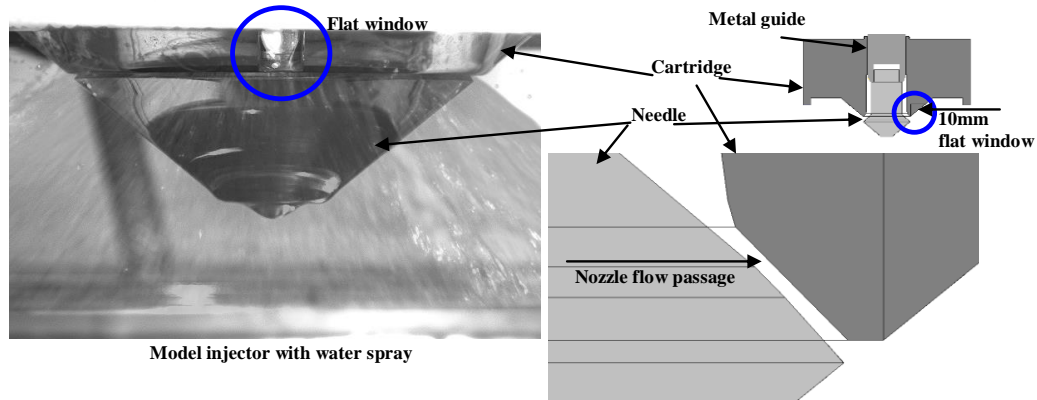**Figure 3:** Model injector set up for injection into air and water.

Figure 4: Flow passage between the needle and the cartridge of the cavitating nozzle.

The injector is an outwards opening piezo injector with a converging-diverging nozzle flow passage close to its exit and a small parallel section in-between where the nozzle seat is as shown in Figure 4; this configuration is referred to as the cavitating nozzle and has an overall nominal cone angle of 90º. The main difference between this design and that used in [16] is the outer surface profile of the needle which has triple angles in the cavitating model and a single angle in the non-cavitating one where the divergence section at the nozzle exit is parallel. In order to prevent image distortion of the nozzle flow due to the strong curvature of the cartridge outer surface, a flat window of 10mm width and 20 mm length (to insure complete viewing of the nozzle seat region) was machined and inserted at the outside surface of the cartridge as shown in Figure 4.

Spray Visualization Setup

Spray images have been taken with a high speed CCD camera (having a 12bit fast shutter Sensicam and a resolution of 1280x1024 pixels) with an exposure time of 0.7-3μs. The camera was fitted with a zoom lens and connected to a PC via an image acquisition card. The PC also had a timer card installed that triggered both the flash lamp illumination and the camera. All internal camera settings were adjustable by the image acquisition software. The spray was illuminated by a Xenon spark light equipped with two flexible optical fibers which increased the effectiveness of the imaging set-up; the spark light intensity was of the order of 200 J/pulse with a pulse duration of 10μs. To visualise the gaseous bubbles inside the nozzle, a zoom lens was used to produce high-magnification two-phase flow images at the nozzle exit.

For the visualisation of the gaseous flow in the nozzle, shadowgraphy was employed so that the presence of the gas phase was identified as black shadow. To relate these occurrences with the spray structure, it was necessary to match forward illumination for the nozzle flow with backward illumination for the spray structure, as shown in Figure 5. This was achieved by using two optical fibres connected to the spark light. A signal is produced by a pulse generator which is triggering both the spark light and the camera. Since the capacitor of the spark light needs 12 seconds to get fully charged, the trigger frequency was set at 0.08 Hz.
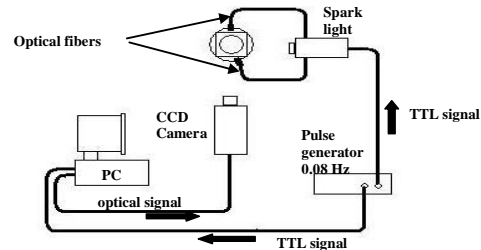

Figure 5: schematic diagram of spark light, camera and PC set up.

In order to understand the dynamic behaviour and temporal evolution of the flow inside the nozzle, a high-speed video recorder was used able to capture up to 40k frames per second (fps). Since, however, at such acquisition rate the spatial resolution of the camera decreases considerably, video images of 27k and 18k frames per second have been recorded with a special resolution comparable to the imaging window. Two halogen spotlights have been used as the continuous light source. The video recorder was triggered by remote control connected to a data store unit and then the images were transferred to the computer for processing. Similar flow conditions were considered to those observed with the Sensicam camera.
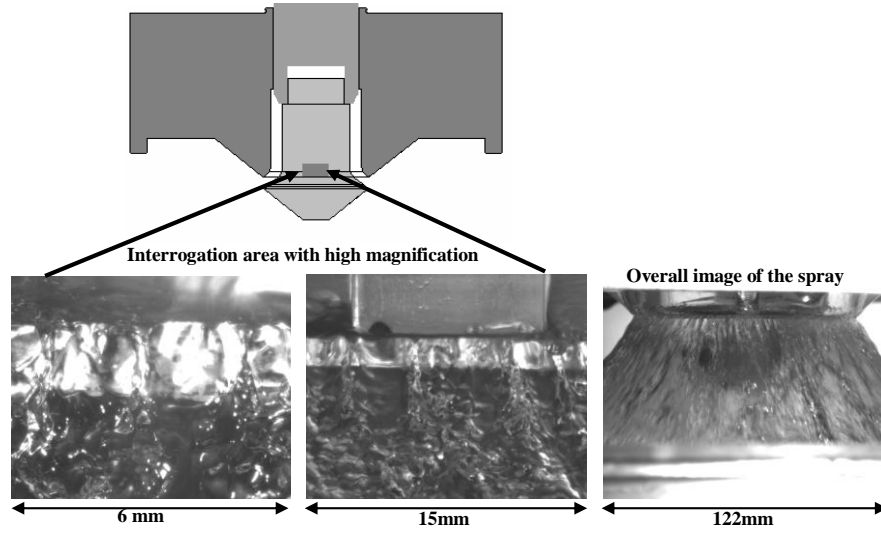
Figure 6: Different image magnification for nozzle flow and overall spray.

With both cameras, in order to fully understand the flow phenomena inside the nozzle, it was necessary to perform imaging using different magnifications. Three levels of magnification with special resolution of 122, 15 and 6 mm were used to visualise the spray, nozzle flow and combined nozzle flow and spray, respectively, as shown in Figure 6. The high magnification images were found to be very useful as they allowed the correlation of the string spray structure downstream of the nozzle with the flow behaviour through the nozzle to be identified.

Valve lift [mm]		Flow Rate		U_{inj} [m/s]		Re	CN
Model	Real size	Model [l/s]	Real [g/s]	Model	Real size		
0.575	0.025	0.7	8.75	5.9	64.7	5383	0.184
0.575	0.025	1.2	15	10.1	111	9228	0.29
0.575	0.025	1.8	22.5	15.17	166	1384	0.474
0.928	0.04	0.7	8.75	3.67	39.7	5393	0.093
0.928	0.04	1.2	15	6.28	68	9246	0.17
0.928	0.04	1.8	22.5	9.42	102	13868	0.31

Table 1: Flow tests conditions and their corresponding values for the real size nozzle.

RESULTS AND DISCUSSION

The spray results presented in this paper were obtained in the enlarged model of a piezo injector incorporating a cavitating nozzle. The results, at different flow rates and needle lifts, showed that cavitation occurred only under certain operating conditions particularly at high flow rates and very low needle lifts, while at other operating conditions gas phase entrainment into the nozzle from outside was observed that had a profound effect on the spray structure. The previous investigation [11] in a non-cavitating nozzle with a parallel nozzle section revealed neither cavitation nor air entrainment taking place in the near nozzle exit under operating conditions similar to the present work.

The results showing air entrainment will be presented first followed by the cavitation results. Measurements were made at two valve lifts of 0.575 and 0.928 mm and at each lift three different flow rates (low, medium and high) were tested (see Table 1). Water was used as the working fluid and was pumped through the enlarged nozzle with an injection velocity of U_{inj} resulting in the same Reynolds number, Re, as that of the real size injector; the calculation of Re is given below together with that of the cavitation number, CN:

$$\mathrm{Re} = \frac{2 \cdot \rho_f \cdot U_{inj} \cdot Lift \cdot \sin\alpha}{\mu_f}$$

$$U_{inj} = Q/A$$

and

$$CN = \frac{P_u - P_d}{P_d - P_v}$$

where ρ_f and μ_f are the liquid density and dynamic viscosity, with the geometric symbols as shown in Figure 7; P_u, P_d and P_v represent the upstream nozzle, downstream nozzle and water vapour pressures, respectively. Given the flow rate, Q, and the flow area, A, at the nozzle seat region, the mean injection velocity and Reynolds number under steady flow conditions can be calculated. Table 1 shows the operating conditions for three flow rates in the enlarged model and their corresponding values in the real size injector.

Spray
Initial observations of the spray presented in Figure 8 show a small sample of the overall structure of the spray emerging from the nozzle at different flow rates and needle lifts. It is evident that the emerging annular liquid jet spray is not uniform and appears to have alternating thin and thick liquid ligaments, with the latter one in the form of strings. It is also clear that this string-type spray structure depends on both needle lift and flow rate, in terms of the surface quality and number of strings. Figure 7(a) shows the effect of the flow rate at full needle lift, revealing a rough spray surface at low flow rates which remained rough as the flow rate was increased until a value of 1.35 l/s when a transition took place to an increased number of strings and a smoother spray surface. The second comparison shows the dependency of this transition to the variation of the valve lift at the high flow rate of 1.80 l/s shown in Figure 8(b). At this flow rate, the results show that it is possible to obtain a rough surface for a lift of 0.57 mm and a smooth surface at the full lift of 0.93 mm. However, the results showed that up to a flow rate of 1.3 l/s the spray surface was always rough independent of valve lift.
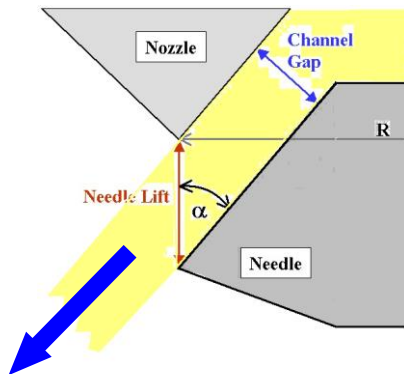

Figure 7: Geometry of the needle and its seat.

Observation of the spray in the new enlarged cavitating model showed a different structure to that observed in the non-cavitating injector [16]. A small sample of the results, presented in Figure 8, clearly show the complex nature of the spray with its many jet like strings which suggests that, apart from ambient effects on the emerging spray, there have to be changes in the flow structure within the annular nozzle passage. Due to the complexity of the spray structure emerging from this injector, the following effects have been investigated. First the internal annular nozzle flow was investigated by visualising the water flow when injected into air and water, and then the spray structure outside the nozzle exit.
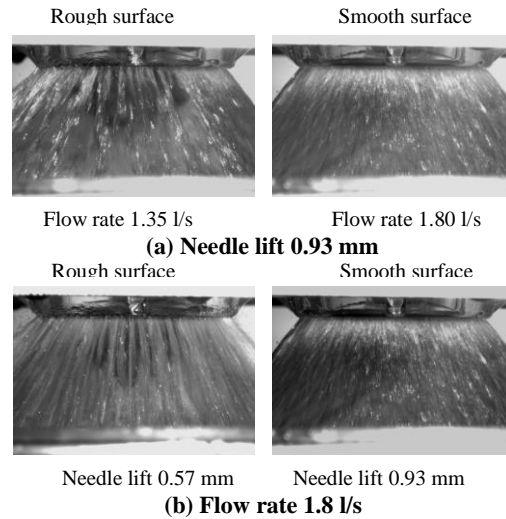

Rough surface   Smooth surface

Flow rate 1.35 l/s   Flow rate 1.80 l/s
(a) Needle lift 0.93 mm
Rough surface   Smooth surface

Needle lift 0.57 mm   Needle lift 0.93 mm
(b) Flow rate 1.8 l/s

Figure 8: Images of string-type spray structure: (a) effect of flow rate at the full needle lift of 0.93mm, and (b) effect of needle lift at a flow rate of 1.8 l/s.

In-nozzle flow
Initial observations, under normal operating conditions, revealed the presence of gas bubbles inside the nozzle passage and to identify the nature of this gas flow closer inspection was needed. A series of highly magnified images of the flow from the nozzle seat area through the designed flat window were obtained and a small sample of them is presented here. Figure 9 shows clearly the presence of gaseous bubbles (the black area) just upstream of the nozzle exit; these gas bubbles were seen at all flow conditions investigated even at a very low flow rate. It was evident that, in all cases, these bubbles were always attached to the edge of the nozzle exit, with no isolated bubbles growing upstream into the nozzle flow passage. This implies that their formation could not take place in the narrow section of the nozzle passage and that they were entrained into the nozzle seat region from outside.

To demonstrate the dynamic behaviour of these entrained gas bubbles, a high speed camera was used and the results are shown in Figure 10; the images are related to the full needle lift of 0.93mm, a flow rate of 1.2 l/s, and a framing rate of 9000fps. Figures 10(a) to (j) show the sequence of the real time images of the nozzle flow with a time interval of 0.55 ms, representing the evolution of the air entrainment as the air is sucked into the nozzle from outside. The arrow in Figure 10(a) indicates the initial position of the developing air entrainment. It was quite rare to capture an

air trap developing in the vicinity of the viewing window, since most of the air traps appeared at the window as soon as the flow was started and, usually moving around the valve seat area. However, the sequence of images in Figure 10 shows clearly the formation of air bubbles taking place at the edge of the nozzle exit. The bubble started to penetrate into the nozzle in Figure 10(b) and grew in time so that at 2.2 ms later, Figure 10(f), the bubble is at its most developed phase; this provides an estimate of the overall time taken for a typical bubble to be fully developed, and is of the order of 2.78ms.
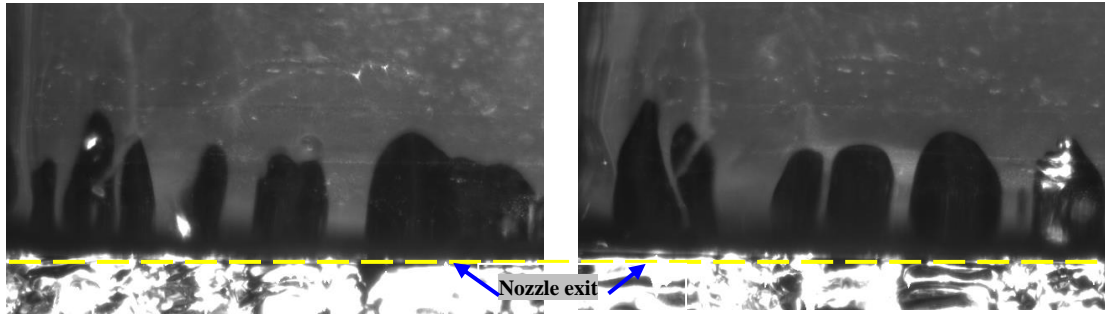

Figure 9: Presence of gas bubbles inside the nozzle flow passage near the exit at a needle lift of 0.57 mm and a flow rate of 0.98 l/s.

(a) frame 67

(b) frame 72

(c) frame 77

(d) frame 82

(e) frame 87

(f) frame 92

(g) Frame 97

(h) frame 102

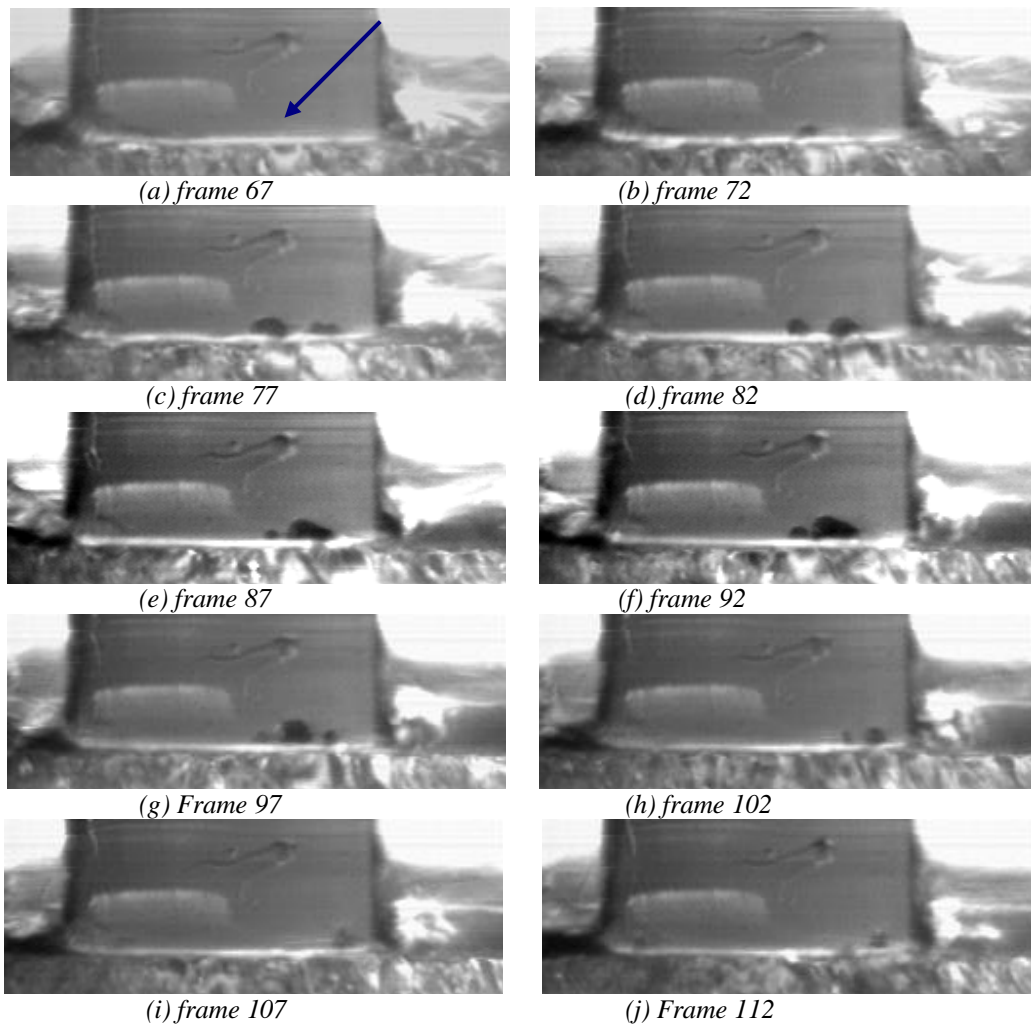*(i) frame 107*

(j) Frame 112

Figure 10: Real time images of evolution of air entrainment into to the nozzle flow passage for a needle lift of 0.93mm and a flow rate is 1.2 l/s; the time sequence between each image is 0.55 ms

The exit flow velocity at this flow condition is 6.2 m/s which gives a mean flow time response of 0.106ms based on $t=G/U_{inj.}$ where $U_{inj.}$ is the mean injection velocity and G is the gap between the needle and the cartridge in the seat region given by G=(needle lift)$cos45°$. This indicates that the flow time response at this flow condition is about 26 times faster than that of the bubble development. This suggests that, for the bubble to be able to penetrate into the nozzle against such a high momentum liquid jet flow, there should be flow separation of the jet from either the cartridge or the needle surfaces close to the exit with a flow time response comparable to that of the bubble development. The bubble formation on the needle or cartridge surfaces has different consequences, especially on the spray cone angle, and this will be discussed later.

In-nozzle flow and spray

After identifying the presence of air bubble entrainment into the nozzle it was decided to visualise the in-nozzle flow and spray simultaneously in order to investigate the direct effect of these bubbles on the emerging liquid spray. This is expected to throw some light on the string formation and also on the spray instability also known as 'flapping'. Initial observations have identified the presence of the latter phenomenon in the form of variations in the spray cone angle so that wide and small spray cone angles could be observed at the same operating point (of valve lift and flow rate). It was found that the occurrence of these wide and small cone angles under the same operating condition was entirely due to in-nozzle flow conditions before switching on the pump. For example, if the flow inside the nozzle passage and upstream of it was full, or partially full, of air pockets then, after switching on the pump, the emerging spray would have a half cone-angle of

approximately 51° which is larger than the nominal value of 45° as shown in Figure 11(a); this is referred to as wide cone-angle. Once created, this flow condition was very stable and could last indefinitely. However, if there was no air trap inside the nozzle, i.e. when the entire volume of the nozzle injector was filled with water, then by switching on the pump the emerging spray would have a half cone-angle of around 41°, Figure 11(b), which is smaller than the nominal value and is referred to as small cone-angle. It was also observed that, under certain conditions (small lift and high flow rate), it was very difficult for the flow to maintain this small cone-angle structure and became unstable, with the spray cone-angle switching from small to large and vice versa.

Based on the results and discussion presented in the preceding paragraphs, it is becoming clear that the presence of the air bubbles entrained into the nozzle is responsible for this instability of the spray cone-angle. To explain the flow mechanism which gives rise to either a small or a wide spray cone-angle, a simple flow model is proposed below in which the existence of different spray cone-angles are linked to the position of the air bubbles with respect to the cartridge or the needle lift. When pockets of air are entrained into the nozzle and depending on the location of flow separation, the air bubbles will be attached to either the needle or the cartridge surfaces. When the bubbles are attached to the needle, then they act as a cushion which deflects the liquid flow outwards, as shown schematically in Figure 12(a), and produces a wider cone-angle. On the other hand, when the bubbles are attached to the cartridge, the flow is deflected inwards producing a smaller cone angle, Figure 12 (b).
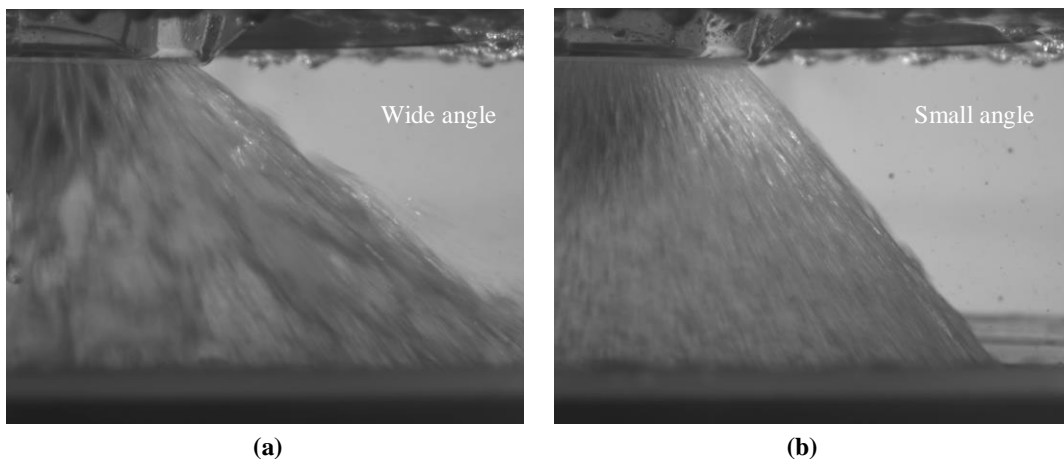

(a)   (b)

Figure 11: Small and wide spray cone-angle for the same operating condition: a valve lift of 0.57mm and a flow rate of 1.0 l/sec.
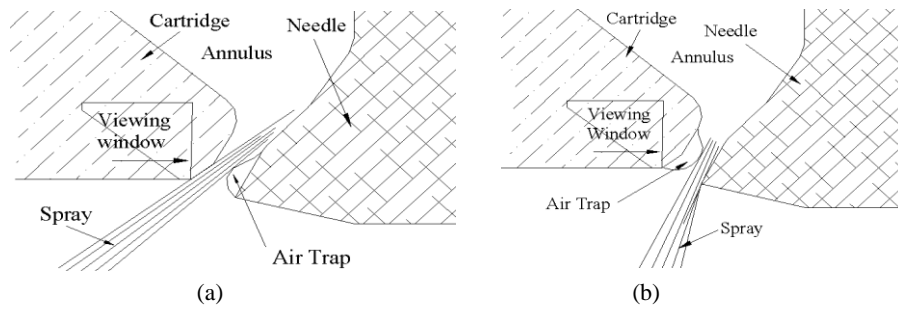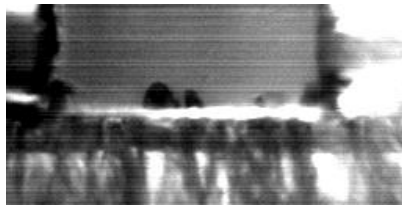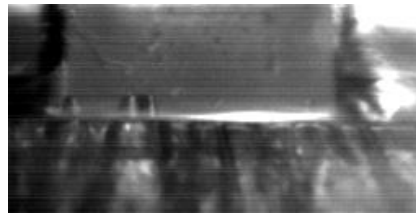
Figure 12: A simple model to explain trends in spray cone-angle (a) air traps attached to the needle causing a wide spray cone-angle and (b) attached to the cartridge causing a small spray cone-angle.
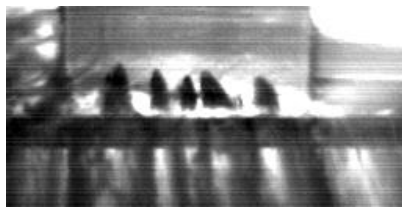
Valve lift 0.575 mm, flow rate 0.7L/s
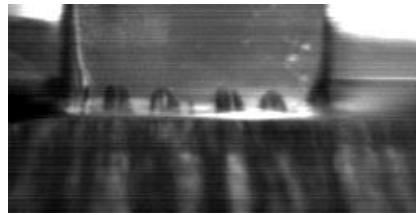

(a) small cone angle

(b) wide cone angle
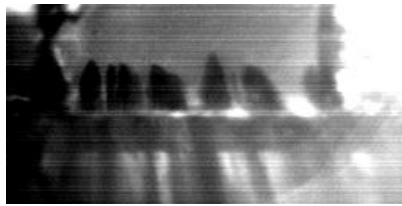
Valve lift 0.575 mm, flow rate 1.2L/s
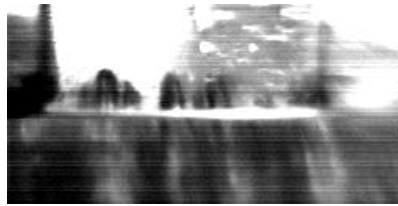

(c) small cone angle

(d) wide cone angle

Valve lift 0.575 mm, flow rate 1.8L/s,

(e) small cone angle

(f) wide cone angle

Figure 13: High-speed video images for comparison between the air bubble formation in the case of small and wide cone-angles.

There are several ways to identify in the images whether the bubbles are attached to the needle or to the cartridge. First, a distinction can be made on the basis of the quality of the bubbles' shadow in the recorded images, which is related to the different type of light (reflection/refraction) as the light path (for different refractive index) in the two cases would be different. In the case of bubbles attached to the cartridge, the observed shadow of the bubbles as viewed from the window were uniformly black while in the case

of bubbles attached to the needle there were some discontinuities in the black shadow with bright spikes, probably attributed to the internal light deflected or refracted by the liquid/gas interface inside the air bubble. These effects can be seen in almost all CCD and video recorded images and Figure 13 provides such a comparison.

Another way to distinguish between the two cases is by measuring the projected length of

bubble penetration into the nozzle from the acquired images. The measurements were made according to the procedure given below and the results are presented in Table 2, which shows clearly that the measured height of the bubble penetration for the wide cone-angle (M) is always lower than those for the small cone-angle (S). Thus, when observing the air bubbles through the viewing window, longer bubble penetration imply bubble attachment to the needle while shorter penetration indicates bubble attachment to the cartridge. From the explanation given below on the RHS of Table 2, it should be emphasised that the true measured value of the penetration length for the wide cone-angle given in Table 2 is W=M+L where L is the needle lift. Another useful and consistent conclusion that can be drawn from Table 2 is that, within the measured range, the lower valve lift always gives longer bubble penetration for both small and wide cone-angles. This suggests that flow separation on either boundaries is taking place closer to the needle seat region; this might be expected as the annular jet thickness at lower lifts is smaller resulting in stronger deceleration (or adverse pressure gradient) close to the boundary when the flow expands in the divergent region of the nozzle.

The height of the bubble penetration also depends on the needle lift and exit liquid velocity, as will be discussed later. But in the case of velocity, in general, it was found that as the velocity becomes higher the pressure drop across the nozzle increases with stronger suction within the separated flow and, therefore, longer penetration of the bubble into the nozzle. However, beyond a certain threshold, the penetration doesn't increase further and additional increase may result in reduction of penetration until the bubbles disappear from the viewing window. This may be due to the fact that the flow with higher momentum expands more rapidly and covers the convergence exit section
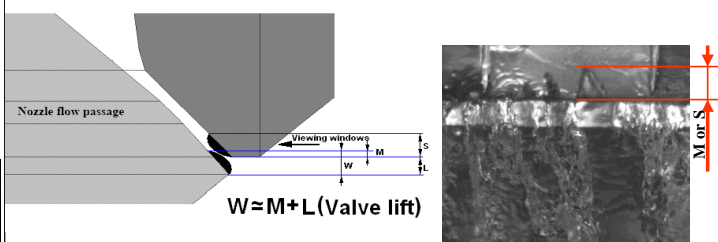
of the nozzle, thus reducing the size of the separated flow.

String Structure Analysis
As mentioned above, an important aspect in the spray characteristics of an outwards opening injector is the presence of a string structure which appears in the form of longitudinal filaments, as can be seen in the magnified image images of Figure 14, and their link to the in-nozzle flow characteristics which is one of the main objectives of the present investigation. It is interesting to note that the string structures are similar to the jet sprays produced by multi-hole gasoline/diesel injectors with their well known 'fish-bone' structure.

A comparison between the real size spray, Figure 14, and the downstream liquid spray of the enlarged model, Figure 15, reveals clearly the presence of longitudinal liquid filaments in both cases. The two magnified images of the string structure in Figure 15 clearly illustrate the direct link between the position of the air bubble inside the nozzle and the liquid filament formed outside the nozzle. The liquid is forced to go around the bubbles and form a liquid jet that exits the nozzle as a liquid string. Immediately below the air bubble, there is a thin liquid coming out of the nozzle which is the liquid flow passing over the bubble. If the air bubble fills the nozzle gap fully, then one would expect in this case that the liquid spray emerges from the nozzle as a series of separated jet flows similar to that of multi-hole nozzle injectors. The results of this investigation under all operating conditions showed no evidence of such spray structure which implies that the air bubbles are always filling the nozzle gap only partially, i.e. they are either attached to the needle or to the cartridge. The emerging liquid spray structure looks like a continuous hollow cone spray with alternating thin, below the bubbles, and thick, between two adjacent bubbles, spray liquid jets.

Bubble penetration (mm)				
Valve Lift / Flow rate	0.92 mm	0.57 mm	0.92 mm	0.57 mm
0.7 l/s	1.0	1.6		1.0
1.2 l/s	1.7	2.0		1.4
1.3 l/s	1.7		0.9	1.6
	Small angle		Wide angle	

W≈M+L (Valve lift)

S = Projected height of the air bubbles measured directly from the images for the small spray cone angle.
M = Projected height of the air bubbles measured directly from the images for the wide spray angle.
W = Projected height of the air bubbles for the wide spray angle; this has been calculated by adding the valve lift to the measured height from the images as this lower part of the gaseous body is hidden by the bright exit gap as shown in above.

Table 2: Air bubble penetration into the nozzle for different operating conditions.
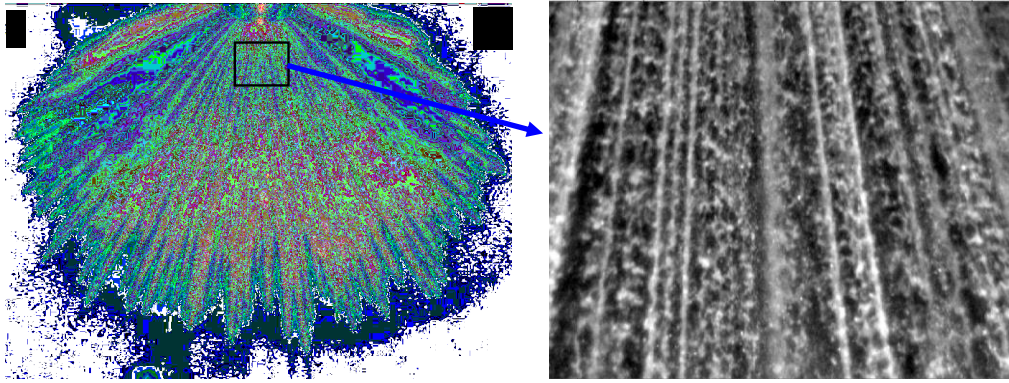
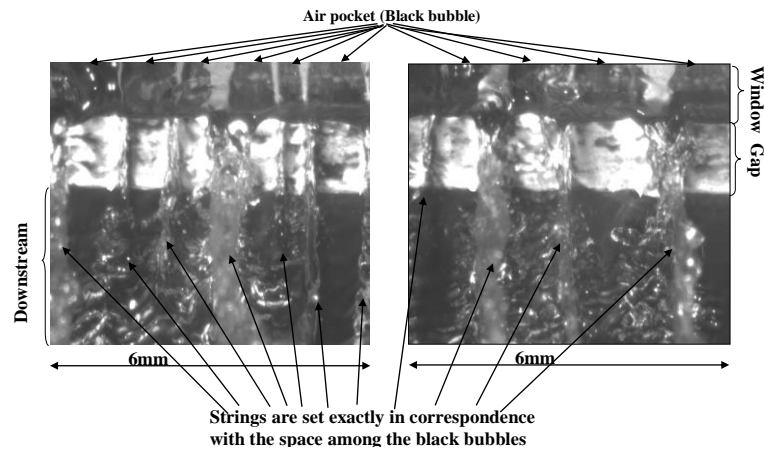**Figure 14:** Magnified image of string structure.

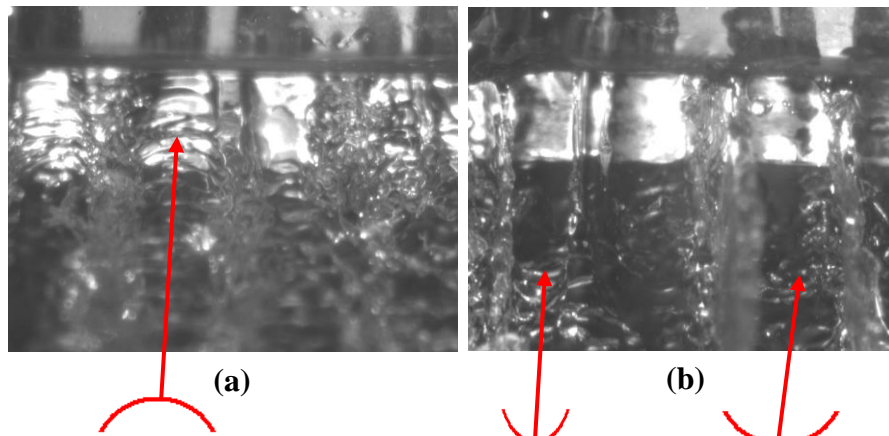**Figure 15:** Correlation between the strings and the in-nozzle air bubble.

Figure 16: Visual differences in the strings structure observed in the images for the (a) wide and (b) small cone-angles at a needle lift of 0.57mm and a flow rate of 1.0 l/s.

Figure 16 presents a third way by which the position of the air bubble with respect to the needle or cartridge surface can be identified; again, as mentioned above, the location of the air bubbles is important as they explain the mechanism which gives rise to either small or large cone-angles. Considering the thin liquid jet flow just outside the nozzle, i.e. when the flow passes over the bubbles, if the bubble is attached to the needle then the part of the flow that passes over the bubble will take the shape of the new boundary (the flow is confined between the bubble and the cartridge) and the result will be a thin spray jet with an outwards convex curvature when the liquid jet emerges from the nozzle exit. On the other hand, if the bubble is attached to the cartridge then the thin liquid spray will look having an inwards concave curvature as the flow confinement this time is between the bubble and the needle. Closer

inspections of images like those presented in Figure 16(a) and (b) reveals that the two types of convex and concave curvature are related to the wide and small spray cone-angles, respectively. It is thus clear that to be able to distinguish between these two types of curvature highly magnified images with high resolution, like that of Figure 16, are required

To clarify the effect of air entrainment on the string structure, it was interesting to observe the spray structure when there was no air entrainment into the nozzle. The results showed that, in the absence of air bubbles, the liquid spray structure downstream of the nozzle exit was completely different with no longitudinal liquid filaments but, instead, a complex structure with corrugated surface; a typical corrugated liquid spray surface in the absence of air bubbles is shown in Figure 17 for the full valve lift at a flow rate of 1.61 l/s. It is clear that there is no air bubble trapped inside the nozzle when viewed through the optical window. It can be argued, however, that there is a small possibility of tiny air bubbles trapped right at the exit of the nozzle, which can not be viewed through the window due to the obstruction by the bottom edge of the cartridge. The corrugated liquid spray emerging from the nozzle has no defined pattern, but right below the nozzle exit-line a pattern of string type structure is visible which may imply the presence of tiny air bubbles in that region. The difference between these strings and those observed in the presence of air bubbles is simply their number, which in this case is much higher. This type of smaller strings is very similar to that observed in a non-cavitating nozzle injector model with a parallel exit passage [16]. However, with the present nozzle and over a short distance away from the exit these string structures become unstable and break down due to the strong interaction with each other, forming the corrugated spray structure. In the non-cavitating nozzle, this breakdown of the strings does not take place and the strings somehow preserve their stability forming the longitudinal strings further downstream.
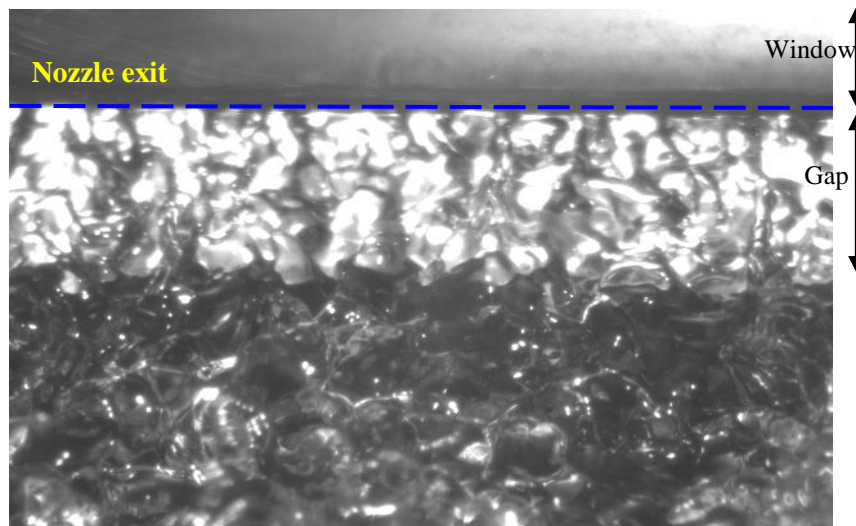

Figure 17: Image of corrugated liquid spray strings when there is no air bubble present in the nozzle at full needle lift and a flow rate of 1.61 l/s.
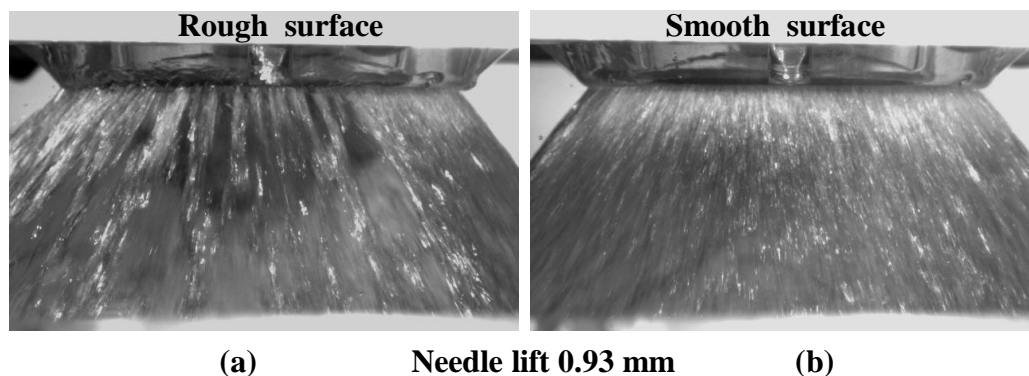

(a) **Needle lift 0.93 mm** **(b)**

Figure 18: Effect of flow rate on surface quality at full needle lift for flow rates of (a) 1.35l/s and (b) 1.8l/s.

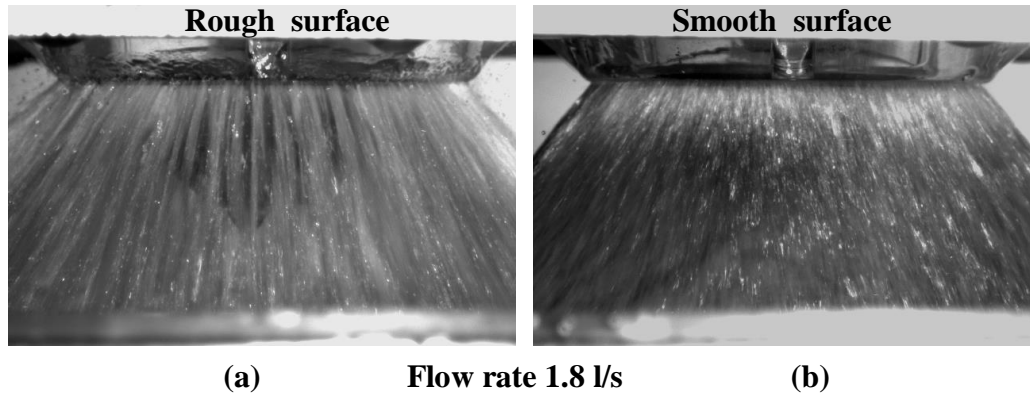| **Rough surface**	**Smooth surface**

(a)   **Flow rate 1.8 l/s**   **(b)**

Figure 19: Effect of needle lift on surface quality at a flow rate of 1.8 l/s for needle lift of (a) 0.57mm and (b) 0.93, full lift.

The transformation of the spray structure from longitudinal ligaments to a corrugated type depends on two parameters, the flow rate (or Reynolds number) and the needle lift. Both cases were examined by keeping one parameter constant and varying the other. In the first case the effect of flow rate was considered at full valve lift and the results are shown in Figure 18 in terms of the overall spray structure. At low flow rates the air bubbles were present inside the nozzle and the annular jet spray exhibited a string type structure with a non-uniform surface, comprising alternating thin and thick ligaments, which is termed 'rough surface'. The spray surface remained rough as the flow rate increased until a value of 1.35 l/s after which the transition to a corrugated surface structure occurred with no air entrainment observed inside the nozzle. As the flow rate increased further the spray structure maintained the same structure.

The second comparison showed the dependency of this transitional spray flow on the variation of the valve lift at a high flow rate of 1.80 l/s as shown in Figure 19. Although at this flow rate the spray structure has already transformed to the corrugated surface (smooth) at the full needle lift, it was possible to obtain a string type spray (rough surface) for a needle lift of 0.57 mm according to Figure 19(a). Based on the measurements of the air bubble penetration presented previously and the related discussion, this effect was expected and suggests that lower needle lifts produce stronger suction (separated flow) than larger lifts. However, the overall results showed that up to a flow rate of 1.3 l/s the spray structure was always of the string type with a rough surface at all valve lifts. Another interesting feature of the string type spray is the dependency of the number of strings on the flow rate and needle lift which will be discussed later.

This can be realised by comparing images of Figure 18(a) and Figure 19(a) that clearly demonstrate that higher flow rates have the effect of increasing the number of strings (i.e. smaller space between two adjacent strings) which suggests that, as the velocity of the liquid increases, there is a breakdown of the large air bubbles into smaller ones. Also the number of the strings at the two needle lifts are different in such a way that smaller lifts produce larger number of strings, but a clear trend can not be identified since the flow rates are different; to clarify this further analysis is required that is presented below. In order to quantify more precisely the effect of flow rate (Reynolds number) and needle lift on the string structure, the average string spacing has been estimated from the magnified images inside the nozzle seat for all flow conditions. In this way it was possible to count the number of air bubbles within a distance of 6 mm. Thus, an average distance between two strings was obtained from each image and then an overall average value, S, based on 40 images was estimated. The results are presented in Figures 20-22 and show the variation of string spacing as a function of Reynolds number, Re, and valve lift.

Figure 20 shows the variation of string spacing with Reynolds number at a valve lift of 0.57mm. The results show clearly that string spacing decreases linearly with an increase in Reynolds number so that S is reduced by about 37% when Re is increased from 5000 to 12000. Since the needle lift has been kept constant, the observed effect is due to a change of the liquid flow rate or velocity. Within the measured range, an empirical relation can be obtained from linear interpolation of the measured data, which relates S to Re and this is given in the graph below.
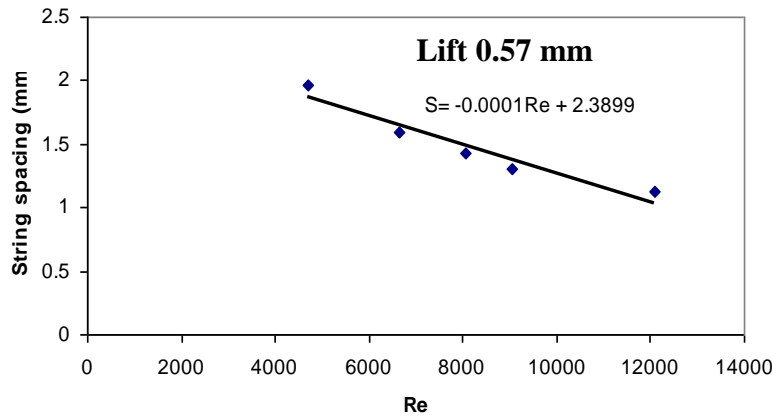
Figure 20: Variation of string spacing as a function of Reynolds number at a lift of 0.57mm.

The variation of S as a function of the needle lift at a constant velocity is presented in Figure 21 and shows a linear increase in string spacing (or decreasing number of strings) with needle lift. Within the measured range, an increase in needle lift from 0.4 to 0.7 mm corresponds to an increase in string spacing of about 16%. A linear empirical relationship has been deduced and is given in the graph. Another representation of needle lifts in terms of S is shown in Figure 22 where the spacing variation is presented as a function of Reynolds number at a constant velocity and for different needle lifts. The results show again a linear relationship between spacing and Reynolds number. Although the variation of string spacing with needle lift, Figures 21 and 22, is not as strong as that with flow rate, the trend is still clear. This suggests that when the liquid velocity is kept constant, reducing the needle lift causes an increase in the number of strings (i.e. reducing S which means that the circumferential size (or diameter) of the air bubbles are smaller at the lower needle lift. This reduction in bubble size also supports the results presented earlier where at lower lifts bubble penetration was longer.
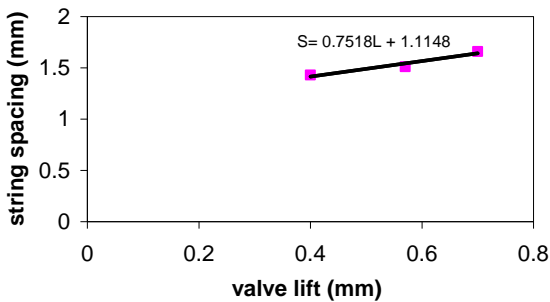
Comparison between the strings spacing, S, of the non-cavitating nozzle injector [16] and the present cavitating nozzle design shows similar dependency of S on flow rate (or injected velocity). The results for the non-cavitating nozzle showed almost no dependency of string spacing with needle lift, while with the present cavitating nozzle the string spacing increased slightly with needle lift as mentioned above. Another difference between the two nozzles is in the number of the formed strings which, as mentioned previously, is much higher with the non-cavitating nozzle by up to 3 times. Finally, the emerging spray structure from the cavitating nozzle looks like a continuous hollow cone spray with alternating thin and thick liquid ligaments forming a string type spray structure with a rough surface (see Figure 23(a)); when at higher flow rates the air bubbles are pushed out of the nozzle, the surface becomes more smooth, Figure 23(b). A similar spray structure was observed in the non-cavitating nozzle with differences in the thickness of the thin and thick liquid ligaments which was much smaller than in the cavitating nozzle, thus forming a much smoother surface, Figure 23(c).
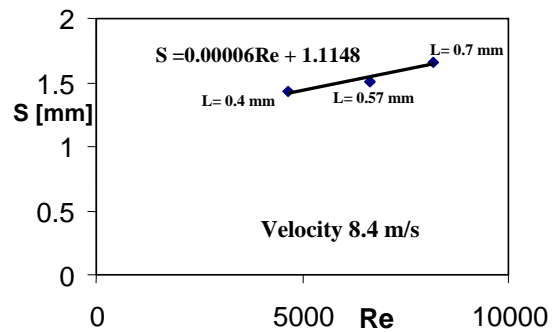

Figure 21: Variation of string spacing as a function of valve lift at a constant velocity of 8.4m/s.

Figure 22 Variation of string spacing as a function of Reynolds number at a constant velocity for different valve lifts.

(a) Cavitating Nozzle
with air bubble; rough surface

(b) Cavitating Nozzle
no air bubble; smooth surface

(c) Non-Cavitating Nozzle
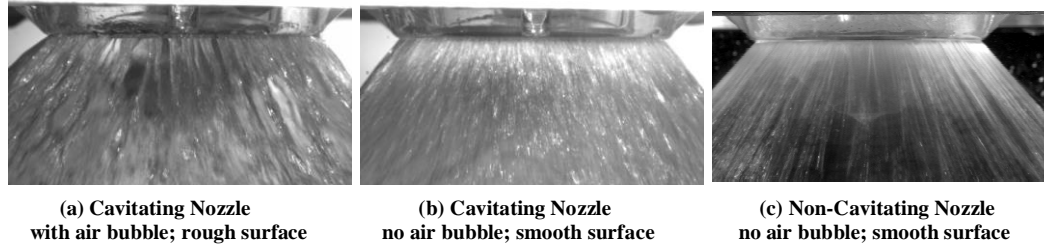**no air bubble; smooth surface**

Figure 23: Comparison of spray surface quality obtained for cavitating and non-cavitating nozzle models.

The present results confirmed that the mechanism of string formation in the cavitating nozzle is related to the existence of the air trapped inside the nozzle diverging section and that the link between these air-bubbles and the emerging liquid spray is well established. In the non-cavitating nozzle, it is expected that a similar mechanism is responsible for the formation of strings, with the entrained air bubbles being much smaller in size while their penetration is restricted to the exit of the nozzle, something that explains the increased number of strings in the non-cavitating nozzle.

Cavitation

There is a need to compare the results obtained for air bubbles entrained into the nozzle with gas vapour produced through the cavitation process. With the present set up for the cavitating nozzle and under all operating conditions, no cavitation was observed due to insufficient pressure difference across the nozzle, due to the pump being not strong enough to create an adequate pressure difference. In order to distinguish between the phenomenon of air entrainment and cavitation, it has been necessary to isolate the nozzle so that no air could be entrained into it. To achieve this, a bottom chamber was added to the cartridge casing to allow injection of water into water, as shown in Figure 3(b).

To initiate cavitation, it was necessary to increase the flow rate and reduce the needle lift in order to increase the pressure drop across the nozzle. After several attempts it proved possible to identify some vapour for a valve lift of 0.5 mm or below; in contrast, air entrainment was observed at much higher lifts and lower flow rates. Apart from using low lifts to increase the pressure difference across the nozzle, it was necessary to connect two pumps in the flow circuit so that the first pump could act as the delivery pump, connected upstream of the nozzle before the flow meter, while the second pump was connected to the exit of the chamber to create suction at the exit of the nozzle. The flow conditions considered here are listed in Table 3.

valve lift [mm]	Flow rate [l/s]	CN	Camera Speed [fps]
0.3	0.80	3.12	27000
0.3	0.80	3.12	18000
0.4	0.94	1.22	27000
0.4	1.12	1.3	27000
0.4	1.12	1.3	18000
0.5	1.05	1.04	27000
0.5	1.34	1.29	27000

Table 3: Flow conditions for the nozzle cavitation case.

As a starting point it was necessary to establish the onset of cavitation and its dependency on parameters such as CN, Re and needle lift. To identify the onset of cavitation, the following procedure was followed since the determination of the occurrence of cavitation onset was quite subjective. Since at the onset of cavitation the number of vapour bubbles is rather small, it proved very difficult to observe them although their presence was quite audible. Then, the decision was taken to define the onset of cavitation at a point when noise was first heard rather than any visual observation. The cavitation number, CN, for different operating conditions was calculated from the relationship given earlier on for three needle lifts of 0.35, 0.4 and 0.5mm. The results of CN as a function of the Reynolds number showed that the inception of cavitation occurred at almost the same cavitation number for all valve lifts and independent of the Reynolds number with an average CN value of 0.53 ± 0.05. From a qualitative analysis within the observed range it is possible to conclude that the onset of cavitation mainly depends on the pressure difference across the nozzle which can be represented by a unique cavitation number.

A typical example of cavitation inside the nozzle is presented in Figure 24. The image clearly shows tiny (like mist) vapour bubbles exiting the nozzle, which suggests that when the pockets of vapour are initiated inside the nozzle they may undergo extensive breakdown within the nozzle passage so that by the time they reach the exit they are completely broken

and appear as mist of vapour at the exit. To gain more insight into the vapour initiation and its development, high magnification images were obtained inside the nozzle through the viewing window.
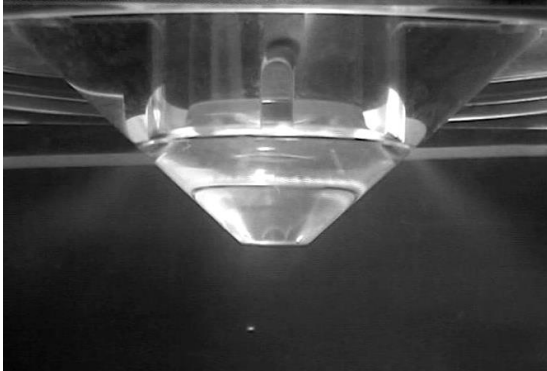

Figure 24: Image of a cavitating jet spray emerging from the nozzle exit at L=0.4 mm, Q=1.12 l/s and CN=1.3.

This phenomenon and its development were visualized in detail through the viewing windows inserted in the cartridge by using the high-speed video recorder. Sample results are presented in Figure 25 and show cavitation development for a needle lift of 0.4mm, flow rate of 0.94 l/s, and a CN value of 3.12 at a frame rate of 18000 fps. The aim of the sequences of images 25(a)-25(n) is to show the location of the initiation of cavitation and its development inside the nozzle. As can be seen, even at this high frame rate, it is very difficult to follow the dynamics of the vapour and an even higher frame rate is required; a speed of 27000 fps was also used, albeit with lower image resolution, but the results proved to be rather similar.
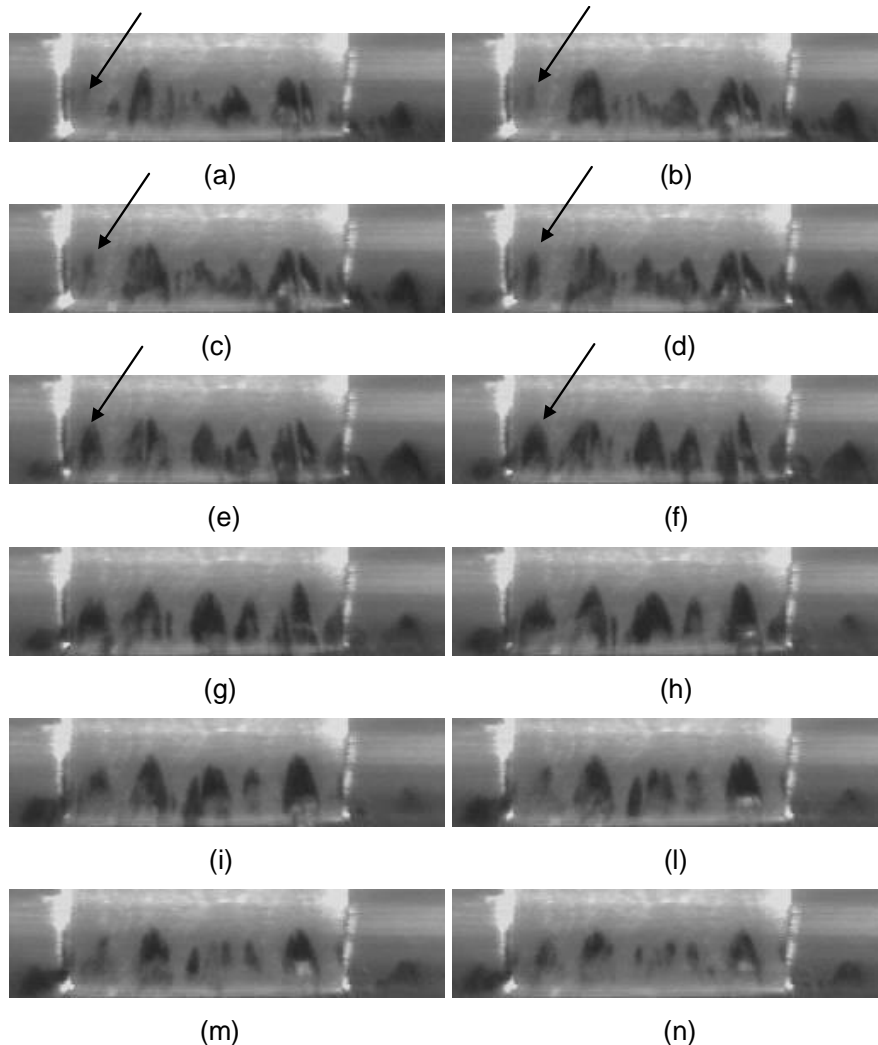

(a)   (b)

(c)   (d)

(e)   (f)

(g)   (h)

(i)   (l)

(m)   (n)

Figure 25: Images of cavitation development inside nozzle seat at L=0.3 mm, Q=0.8 l/s, CN=3.12 and a frame rate of 18000 fps.

From the presented time sequence, it was possible to estimate a typical time response in which the vapour pockets emerge and disappear; this time response is useful for the behaviour of isolated pockets of vapour that can be identified, but is not representative of the dynamics of the vapour development and should be treated with care. The arrow in image 25(a) indicates the area where cavitation is about to initiate and develop. As soon as vapour pockets reach a certain size, they are quickly broken down and convected downstream, either disappearing completely or disintegrating into a smaller number of pockets (in a cascade process) which tend to move sideways. The mean flow velocity in the nozzle for the case shown in Figure 25 is 12.9m/s. Therefore, applying the same procedure to that of air entrainment it was found that the mean flow time response was of the order of 0.023ms. This suggests that to resolve the motion of the vapour, the frame rate has to be larger than 44,000 fps. The time response from the emerging pockets of vapour bubbles until their extinction was estimated to be about 0.66ms (within 12 frames at a camera speed of 18000fps), which is much faster than that of the air entrainment by around 4 times, and much slower than the flow time response by about 28 times. This suggests that, as soon as vapour is formed, bubbles will be subjected to high velocity flow with strong shearing across the nozzle section which will eventually deform, break up and convect them downstream fast enough so that they emerge from the nozzle in a mono-dispersed vapour cloud like that of Figure 24. The presence of vapour inside the nozzle at this flow condition with a cavitation number of 3.12, Figure 25, was continuous and the nozzle can be considered to be at a full cavitating state.

From the images, it is also clear that cavitation (unlike the phenomenon of air entrainment) forms and develops away from the nozzle exit, in and in particular close to the nozzle seal band. It initiates at a point and disperses quickly downstream forming a triangular shape with its apex being the location of the initiation of cavitation. Dark areas in the flow indicate where the vapour bubbles are forming as a result of the boiling process. Closer inspection of the images revealed that the starting point of cavitation was along a horizontal line across the window which coincided with the edge dividing the constant (parallel) nozzle passage and the beginning of the diverging section of the nozzle exit, as shown in Figure 4. This was expected since, as the flow undergoes extensive acceleration in the converging section and into the parallel section of the nozzle, the pressure drops progressively with minimum pressure towards the end of the parallel section and just upstream of the converging section. The results of Figure 25 suggest that this pressure drop is large enough to bring the liquid pressure below the liquid vapour pressure and initiate cavitation.

(a) Air bubble entrainment: Q=0.98 l/s; L=0.57 mm; CN=0.3; frame rate 9000 fps.

(b) Cavitation: Q=0.8 l/s; L=0.3 mm; CN=3.12; frame rate 18000 fps.
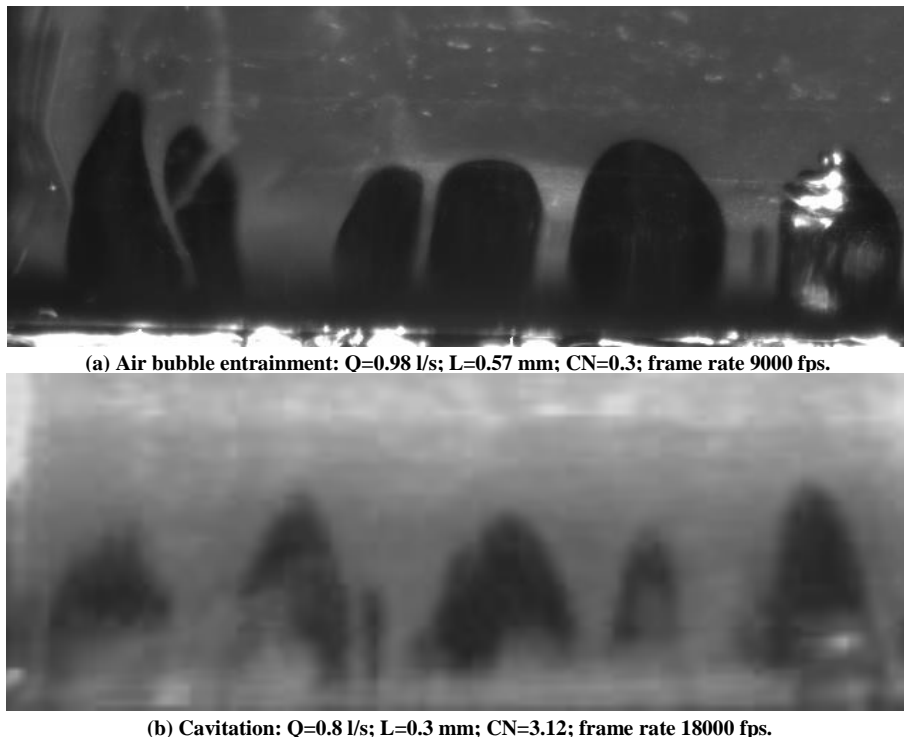
Figure 26: Close up Comparison between the air bubbles entrainment and cavitation structure.

A comparison between the air-entrained and the cavitation bubbles is presented in Figure 26 and clearly shows that a different structure exists between the two phenomena. The effect of time scale is obvious with a sharp image of the air bubbles which confirms the singularity of the air trapped; this suggests that the frame rate adopted was enough to freeze the bubble movement. This, however, is not the case for the vapour bubbles which are very difficult to be distinguished from each other, highlighting the problem mentioned earlier about the need for a much higher frame rate in order to capture the dynamics of the vapour bubbles. Nevertheless, the close-up image clearly shows the presence of vapour pockets forming a triangular shape structure with onset of cavitation at its apex.

The initiation of cavitation can also be observed in Figure 27 which represents another sequence of cavitation at a larger needle lift of 0.4mm than that of Figure 25 and at a much smaller cavitation number, CN, of 1.2. At this CN value cavitation has just started and is in a transient state. Images 27(a)-27(x) show clearly the initiation of the cavitation bubbles within the nozzle seat which then break, disperse and move fast towards the nozzle exit. Since the pressure is unstable and varies around the liquid vapour pressure, P_v, as soon as the pressure recovers and goes above P_v cavitation stops causing intermittent cavitation. The results of Figure 27 show that the time between the onset of cavitation until its extinction later on was about 0.8ms, which is longer than that of Figure 25, as expected.

(a)   *(b)*   *(c)*   *(d)*

(e)   *(f)*   *(g)*   *(h)*

(i)   *(j)*   *(k)*   *(l)*

(m)   *(n)*   *(o)*   *(p)*

(q)   *(r)*   *(s)*   *(t)*

(u)   *(v)*   *(w)*   *(x)*

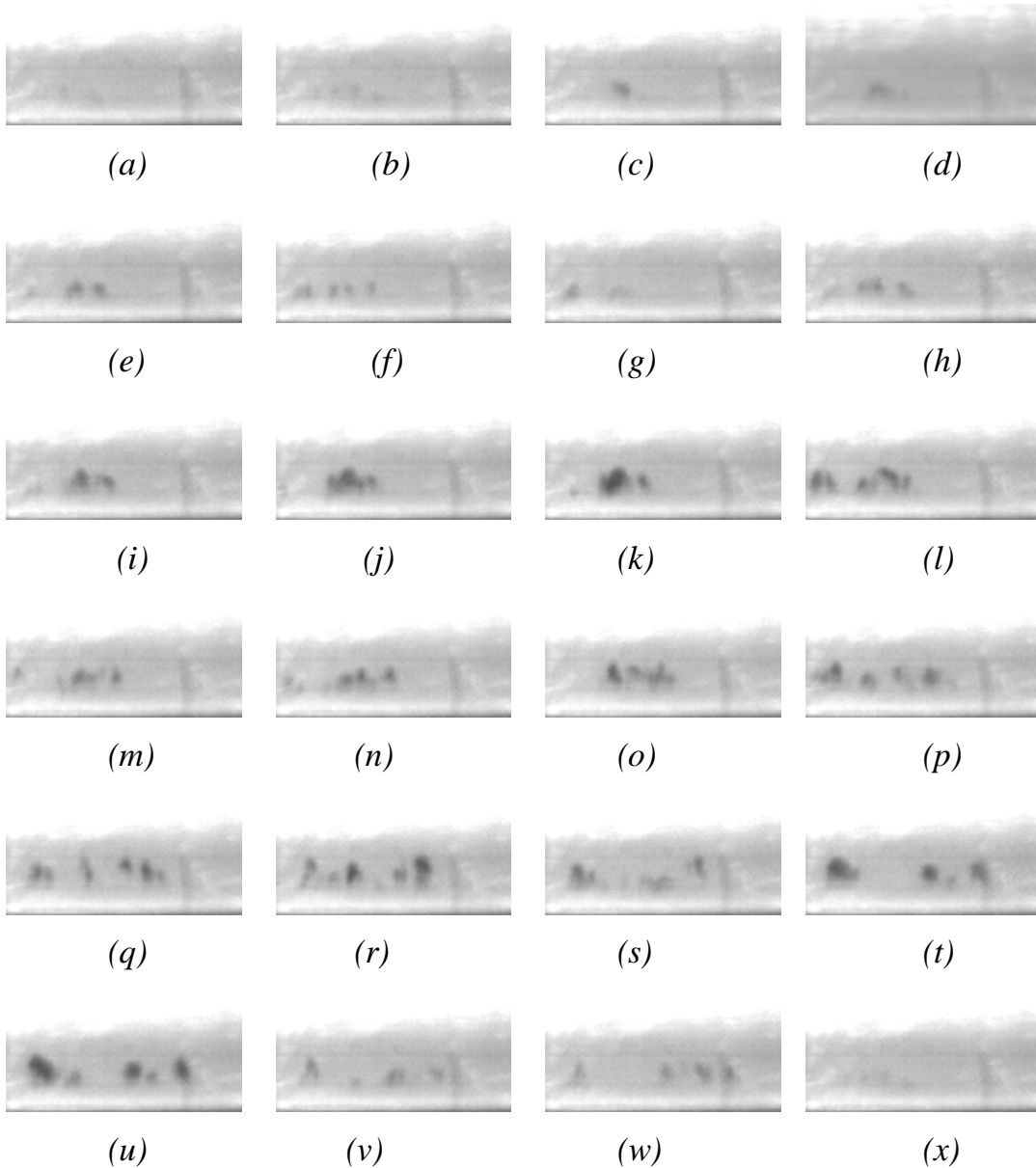**Figure 27:** Images of cavitation development inside nozzle seat at L=0.4mm, Q=0.94l/s, CN=1.22 and frame rate of 27000 fps.

Another distinctive feature of the cavitation bubbles is the detachment of the vapour bubbles from the nozzle exit line as can be seen from the images of Figures 26(b) and 28(b) and the schematic presentation. This feature is in contrast to the entrainment air-bubbles which were found to be always attached to the nozzle exit line. This difference in the behaviour of cavitation and air bubble entrainment can be used to distinguish the two phenomena apart from their appearance which is uniformly dark in the case of the air bubbles entrainment.

It was impossible to assess the quality of the spray under cavitating conditions because injection was into water. Also, as mentioned before, it was very difficult to initiate cavitation when injecting into air. However, using the two pumps in series to boost the delivered pressure of the liquid into the nozzle, a condition that satisfied the cavitation criteria, i.e. CN of 1.6 for a needle lift of 0.57mm; the results are presented in Figure 29. Although the phenomena of air entrainment and cavitation were described before separately, we cannot exclude the case of the two phenomena taking place at the same time creating a multi-phase flow condition that is normally referred to as 'super cavitation'.
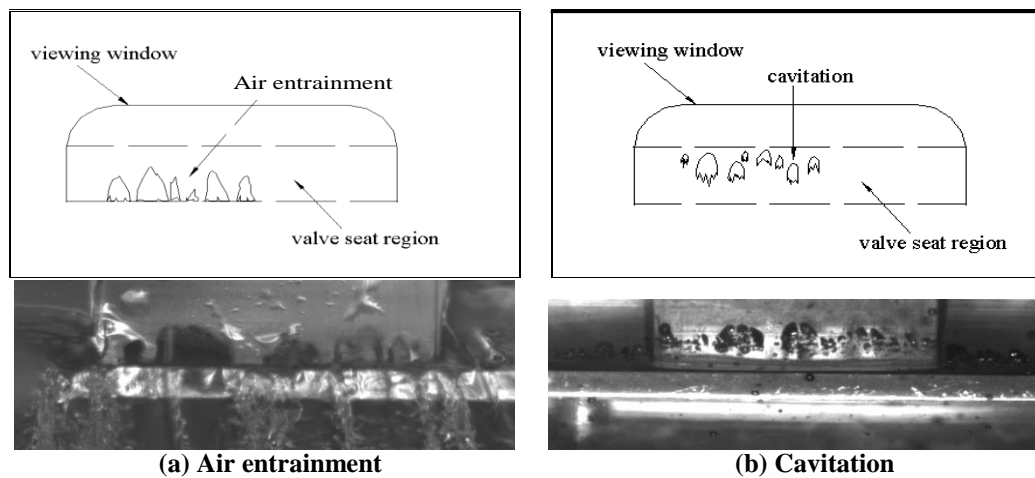

(a) Air entrainment   (b) Cavitation

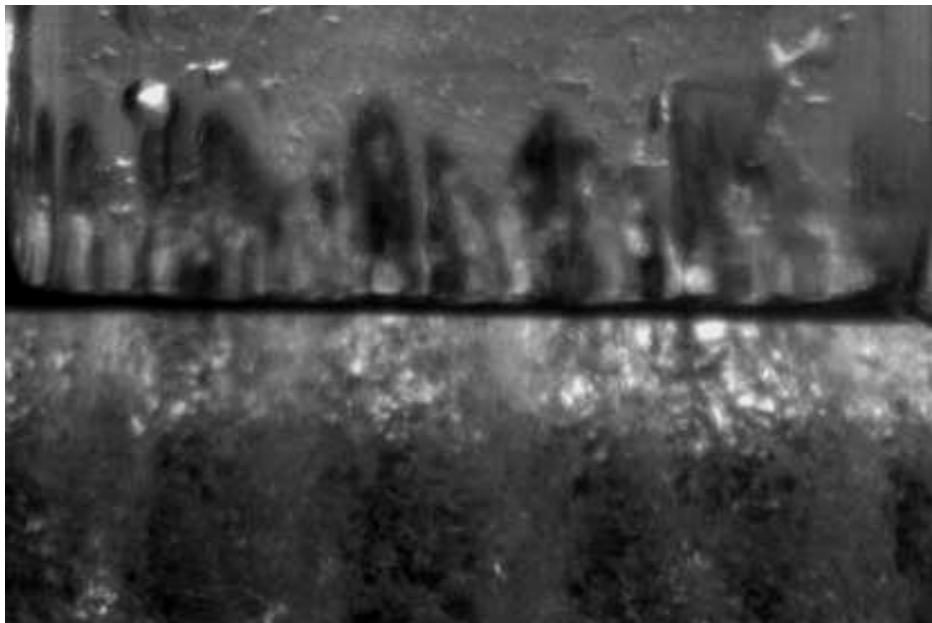**Figure 28:** Schematic presentations of air entrainment and cavitation.

Figure 29: Image of spray and in-nozzle flow at a valve lift of 0.57mm, a flow rate of 2.6 l/s and a CN of 1.6.

The results clearly show the immediate effect of increased velocity and pressure drop across the nozzle in terms of a significant increase in the spray atomisation downstream of the nozzle exit, by comparing those of Figures 15 and 16, so that the thin liquid ligaments below the air pockets are almost fully broken and the same can be seen on the outer surface of the thick ligaments. The overall spray structure now seems more similar to that observed in the real size injector. The flow structure inside the nozzle shows the presence of air entrained bubbles with a sharper black shape shadow and their attachment to the nozzle exit-line. Also, the presence of brighter and fizzy colour shadows is evident which resembles those of cavitation vapour clouds that rapidly disperse. The presence of these two phenomena and the increase in the relative velocity between the liquid flow and the air outside the injector that gives rise to higher Weber numbers and therefore enhanced atomisation, are clearly evident in the image.

CONCLUSIONS

The transparent enlarged nozzle model of an outwards opening piezo-injector for gasoline direct injection engines proved to be an extremely useful tool in understanding the internal nozzle flow patterns and two-phase flow phenomena such as air entrainment and cavitation. The in-nozzle flow visualisation was achieved with a high-resolution CCD camera coupled with a high-speed digital video technique. The most important findings can be summarized as follows:

1. Spray visualization of the cavitating nozzle revealed the presence of gas-phase in the near nozzle exit region which could either be cavitation, under conditions where the pressure drop across the nozzle gave rise to high cavitation numbers of the order of 1.1 and above, or air entrainment into the nozzle due to liquid flow separation from the needle or cartridge surfaces; the latter occurred under most operating conditions and cavitation numbers well below 1.

2. Cavitation and air entrainment proved to be two separate phenomena occurring at different operating conditions with a different structure and dynamic range.

3. In the case of air entrainment, the emerging spray can have two distinct large and small cone-angles according to the attachment of the air bubbles to the cartridge and needle surfaces, respectively, in the near nozzle exit plane.

4. The surface spray structure at these two cone-angles comprised longitudinal strings due to the profiling effect of the liquid flow around the air pockets; the spray thickness downstream of the air pockets was thin whereas the spray below the gap between the two adjacent air bubbles was thicker.

5. Although a similar structure has been observed in the real size injector, it is still not possible to speculate that air entrainment is the only mechanism responsible for the string type spray structure since a finer string structure has been observed in a non-cavitating nozzle. In the non-cavitating geometry, however, it can be argued that smaller size bubbles can be generated at the exit of the nozzle that cannot penetrate upstream into the nozzle due to the geometric restriction, thus unable to initiate finer strings.

6. Entrained air bubbles were always present in the nozzle at needle lifts of 0.57 and below at all flow rates; however, at the full needle lift of 0.93mm, there was a sudden end to air entrainment at the critical flow rate of around 1.3 l/s. This suggested that the flow beyond this critical flow rate became unstable and expanded to fill the diverging section of the nozzle inhibiting flow separation locally.

7. Initiation of cavitation in the examined nozzle geometry and with the present set up proved possible for needle lifts of 0.57mm and below with full cavitation occurring towards the lower range of needle lifts. After their inception, vapour pockets quickly disintegrated, dispersed and convected downstream towards the nozzle exit forming a triangular shape of the vapour with its apex being the point of inception of cavitation close to the seal band of the nozzle.

8. The dynamics of vapour pockets were found to be much faster than those of air entrained bubbles, requiring a higher frame rate camera.

9. Limited tests at low lifts and very high flow rates, where air entrainment and cavitation bubbles occurred simultaneously, revealed that the main mechanism for string structure of the spray was still the air entrained bubbles, but the presence of cavitation at high liquid velocities enhanced cavitation to levels so that the string spray structure became similar to that of the real size injector.

10. Apart from air entrainment, there are other mechanisms that might either hinder or enhance the formation of a string spray structure like the balance of dynamic and surface tension forces and the aerodynamic force due to the induced air recirculation just outside the nozzle exit.

ACKNOWLEDGEMENT

REFERENCES

1. Wirth, M., D. Zimmermann, R. Friedfeldt, J. Caine, A. Schamel, M. Davies, G. Peirce, A. Storch, K. Ries-Müller, K.P. Gansert, G. Pilgram, R. Ortmann, G. Würfel, J. Gerhardt, *A Cost Optimised Gasoline Spray Guided Direct Injection System for Improved Fuel Economy, Seminar on Fuel Economy and Engine Downsizing.* Institution of Mechanical Engineers, One Birdcage Walk, London, 13 May 2004.

2. Iwamoto Y., K. Noma, O. Nakayama, T. Yamauchi and H. Ando, *Development of gasoline direct injection engines.* SAE Paper 970541, 1997.

3. Nouri, J.M., N. Mitroglou, Y. Yan and C. Arcoumanis, *Internal flow and cavitation in a multi-hole injector for gasoline direct injection engines.* To be presented in SAE 2007, 2007.

4. Mitroglou, N., J.M. Nouri, Y. Yan, M. Gavaises and C. Arcoumanis, *Spray structure generated by multi-hole injectors for gasoline direct injection engines.* To be presented in SAE 2007, 2007.

5. Birth, I.G., M. Rechs, U. Spicher, and S. Bernhardt, *Experimental Investigation of the In-Nozzle Flow of Valve Covered Orifice Nozzle for Gasoline Direct Injection.* 7th Int. Symp. Internal Combustion Diagnostics. 2006, pp. 59-78, Kurhaus Baden-Baden.

6. Mitroglou N, *Multihole Injectors for Direct-Injection Gasoline Engines, PhD Thesis in preparation*, City University London, UK, 2006.

7. Xu, M. and Markle L.E., CFD development of spray for an outwardly opening direct- injection gasoline injector., SAE Paper 980493, 1998.

8. Shelby, M.H., B.A. VanDerWege, and S. Hochgreb, *Early spray development in gasoline direct-injection spark-ignition engines.* SAE 980160, 1998.

9. Nouri, J.M. and J.H. Whitelaw, *Impingement of gasoline sprays on angled plates. Atomization and Sprays*, 2006: **16**(6): P. 705-726.

10. Abo-Serie E., C. Arcoumanis and M. Gavaises, *Spray characterisation of swirl pressure atomizers for G-DI engines: phase doppler measurements. ILASS-Europe*, Darmstadt, Germany, 11-13 Sept., 2000.

11. Nouri J.M. and J.H. Whitelaw, *Effect of chamber pressure on the spray structure from a swirl pressure atomiser for direct injection gasoline engines. ICOLAD 2002*, London, 2002.

12. Nouri J.M., M.A. Hamid, Y. Yan and C. Arcoumanis, *Spray characterization of a piezo pintle-type injector for gasoline direct injection engines. ICOLAD 2005*, London, 2005.

13. Mansour, A. and N. Chigier, *Dynamic behavior of liquid sheets. Phys. Fluids A*, 1991: **3**(12): p. 2971-2980.

14. Arai, T. and H. Hashimoto, *Disintegration of a thin liquid sheet in a cocurrent gas stream. ICLASS-85*, London, UK, 9-10 July, 1985.

15. Cavalho, I.S., Heitoyr and D. Santos, *Liquid film disintegration regimes and proposed correlations, Int. J. of Multiphase flow*, 2002: **28**, p. 773-789.

16. Nouri J.M., E. Abo-Serie, A. Marchi, N. Mitroglou and C. Arcoumanis, *Internal and near nozzle flow characteristics from an enlarge model of an outward opening gasoline direct injector. ICOLAD 2005*, London, 2005.

17. M. Gavaises, S. Tonini, A. Marchi, A. Theodorakakos and D. Bouris, *Modeling of internal and near-nozzle flow of a pintle-type outward opening piezo-injector. To be appear in J Engine Research,* 2006.

18. Tonini S. *Multi-phase flow modelling of fuel injection processes in direct injection diesel and gasoline engines. PhD Thesis in preparation*, City University London, UK, 2006.